Journal of Solid State Chemistry **161,** 294–299 (2001)
doi:10.1006/jssc.2001.9312, available online at http://www.idealibrary.com on IDEAL®

Conductivity and Magnetic Properties of New *Ln*MnO_3 Derivatives

P. Martín,* A. I. Ruiz,* J. Campo,† M. L. López,*,[1] M. L. Veiga,* and C. Pico*

*Departamento de Química Inorgánica I, Facultad de Ciencias Químicas, Universidad Complutense, 28040 Madrid, Spain; and
†Institut Max Von Laue — Paul Langevin (ILL), 38042 Grenoble Cedex 9, France

Received February 6, 2001; in revised form July 3, 2001; accepted July 12, 2001

The new phases of composition $Ln_{1.33}Na_xMn_xTi_{2-x}O_6$ (Ln = Pr, $x = 0.66$; Ln = Nd, $x = 0.66$ and 0.55), derived from $LnMnO_3$ by partial substitution of Mn^{3+} by Ti^{4+} and Na^+, are reported. Powder neutron diffraction data were used to refine the crystal structures and to analyze the ferromagnetic interactions. These phases can be described as orthorhombic perovskites, space group *Pbnm*, in which *A*(*Ln*, Na) and *B*(Mn, Ti) cations are disordered at random. Conductivity results are attributed to an electronic contribution and the activation energies are relatively low, about 0.3 eV. © 2001 Academic Press

Key Words: **semiconductors; magnetic behavior; perovskites.**

INTRODUCTION

Perovskite-type and related oxides of the first transition metals have long been of interest for their electronic, magnetic, and many other properties. These compounds can exhibit metallic conductivity and metal-to-insulator (M–I) transitions that in most cases depend on temperature, pressure, or small chemical changes. More noticeable properties were also found as superconductivity in copper oxides and ferromagnetic metallic state in manganese oxide perovskites, associated with colossal magnetoresistence (1, 2). Both magnetic and transport properties in the ABO_3 perovskite-type compounds are closely related to their crystal structure. In order to explain the associated physical properties, relationships between composition and structure are usually established using the formal oxidation state of the transition metal and the tolerance factor. Recently, a third factor related to the effect of disorder due to the disparity of individual *A* cation radii is proposed to be taken into account (3).

An important representative of the manganese oxides is $LaMnO_3$ that shows antiferromagnetic and insulator properties. From the electronic point of view, an orbital ordering is stabilized in this phase by means of the cooperative Jahn–Teller effect breaking the electronic configuration ($t_{2g}^3eg^1$) of Mn^{3+} and this ordering seems to be responsible for a phase transition at about 873 K. In the low-temperature (O′-orthorhombic) phase a Jahn–Teller distortion superimposed onto the cooperative MnO_6 rotations takes place, whereas in the high-temperature (O-orthorhombic) phase only the rotations occur. On the other hand, at higher temperatures (near to 1000 K) the system undergoes a transformation from O-orthorhombic to rhombohedral, which is similar to other structural changes that take place at elevated temperatures in some related systems (4).

In this sense, we have recently reported (5) some results on the structure and electrical behavior of the series $La_{1.33}Na_xMn_xTi_{2-x}O_6$ that formally derives from the parent compound $LaMnO_3$ by substitution of Mn^{3+} by Ti^{4+} and Na^+ cations. The former (Ti^{4+}) cations occupy the *B* sites and the latter (Na^+) are located on the partially vacant *A* sites in these perovskite-type compounds, together with the Mn and La cations, respectively. The present paper deals with the structural characterization by *X*-ray and neutron diffraction as well as the conductivity and magnetic properties of the new phases $Ln_{1.33}Na_xMn_xTi_{2-x}O_6$ (Ln = Pr, Nd). General features are discussed in comparison with the above system.

EXPERIMENTAL

Polycrystalline samples $Ln_{1.33}Na_xMn_xTi_{2-x}O_6$ (Ln = Pr, Nd; $\frac{2}{3} \geq x > 0$) were prepared by the "liquid mix" technique (6) starting from stoichiometric amounts of $C_5H_{21}O_6Mn$, $NaNO_3$, TiO_2, and Pr_6O_{11} or $Nd(NO_3)_3 \cdot 6H_2O$, respectively, as described elsewhere (7). Each mixture was preheated in an alumina crucible at 513 K for 48 h, followed by a further thermal treatment at 723 K for 72 h. Finally, the samples were heated in air at temperatures ranging between 1073 and 1173 K for several days.

The Mn^{3+}/Mn^{4+} ratio in the samples was obtained by redox titration using an excess of $FeSO_4$ solution and back titration with $KMnO_4$, being dissolved the samples in H_2SO_4/H_2O (50/50). A known amount of $FeSO_4$ was

[1]To whom correspondence should be addressed. E-mail: marisal@eucmax.sim.ucm.es

0022-4596/01 $35.00

introduced into the sample solution and the excess was determined by standard $KMnO_4$ solution to give the total manganese and the possible Mn^{4+} content has been determined by the procedure described in Ref. (8).

X-ray powder diffraction patterns were recorded with a Siemens Kristallofex diffractometer powered with a D-500 generator using Ni-filtered Cu$K\alpha$ radiation and a 2θ step size of 0.05° with a counting time of 12.5 s for each step. The goniometer was connected to a PC controlled by the commercial program PC-APD (Analytical Powder Diffraction Software, 4.0e). The Rietveld profile analysis method (9) was applied to refine the X-ray diffraction data.

Neutron powder diffraction patterns were recorded at room temperature on the D1A high-resolution powder diffractometer ($\lambda = 1.9110$ Å) at the Institut Laue–Langevin (Grenoble, France). The neutron patterns were also analyzed using a Rietveld profile analysis method. The multidetector D1B powder diffractometer with a wavelength of 2.52 Å was used for thermal patterns in the 1.5–300 K temperature range.

Electrical measurements were carried out using a Solartron 1260 impedance gain phase analyzer with a frequency range of 0.1 Hz–10 MHz. The pelletized samples were sintered in air at temperatures ranging between 973 and 1073 K for several hours. Blocking electrodes were deposited on both sides of the pellets by platinum paint and resistance values were derived from the complex impedance plane diagrams. Also, measurements in d.c. were carried out using a two-probe technique.

Magnetic measurements were obtained in a SQUID (Quantum Design, MPMS-XL model) with a sensitivity of 10^{-10} emu in the 2–300 K temperature range, applying a field of 1000 Oe.

RESULTS AND DISCUSSION

Chemical analysis of the title compounds gave the Mn^{3+} and Mn^{4+} content in each sample that are believed to be reliable to about 5%. A detectable amount of Mn^{4+} of the order of 15% was found only in the $x = 0.55$ compound (that is, 0.47 Mn^{3+} and 0.08 Mn^{4+}). As occurs in related systems, e.g., in $LaMnO_3$ (10), the perovskite structure is not able to accept an excess of oxygen in interstitial sites, and the more reliable compositions for these phases are: $Na_{0.66}Ln_{1.33}Mn_{0.66}Ti_{1.34}O_6$ ($x = 0.66$; Ln = Pr, Nd) and $Na_{0.55}Nd_{1.33}Mn_{0.55}Ti_{1.45}O_6$ ($x = 0.55$), although a little proportion of cation vacancies are necessary to preserve the crystal electroneutrality.

X-ray diffraction data confirmed that single phases were obtained and all the reflections were indexed in a primitive orthorhombic cell (s.g. *Pbnm*) whose parameters are related to the cubic perovskite parameters (a_p) as follows: $a_o \sim b_o \sim \sqrt{2}\, a_p$ and $c_o \sim 2a_p$.

The structure refinements for the $Pr_{1.33}Na_{0.66}Mn_{0.66}Ti_{1.34}O_6$ compound were carried out separately from X-ray and neutron diffraction. On the basis of the good agreement between both results, this structural model was chosen for all compositions whose XRD results will be discussed. Final refinements were obtained assuming a disordered arrangement of Mn^{3+}/Ti^{4+} cations on the octahedral B sites; the Ln^{3+}/Na^{+} cations and vacancies were located at random over the A sites. Figure 1 shows the observed and calculated neutron diffraction profiles for $Pr_{1.33}Na_{0.66}Mn_{0.66}Ti_{1.34}O_6$ and Table 1 gathers the crystal data and agreement factors. A selection of bond lengths and angles are listed in Table 2, which shows the structural distortions also encountered in other perovskite-related materials (5).

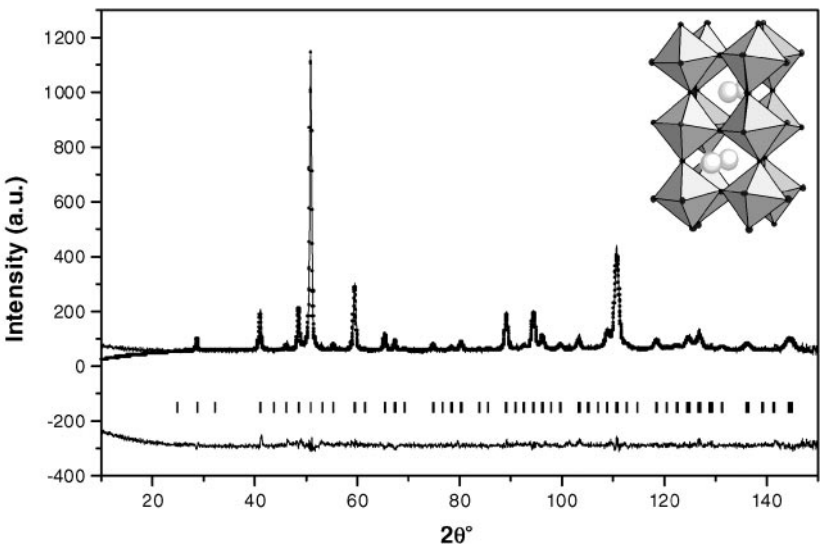

FIG. 1. (full line) Calculated and (dots) observed ND patterns for $Pr_{1.33}Na_{0.66}Mn_{0.66}Ti_{1.34}O_6$ and structural model (inset).

TABLE 1
Refined Atomic Positions, Lattice Parameters, and *R*-Factors for $Ln_{1.33}Na_xMn_xTi_{2-x}O_6$, Obtained by X-ray Diffraction (XRD) and Neutron Diffraction (ND)

		Pr 0.66 (ND)	Pr 0.66 (XRD)	Nd 0.66 (XRD)	Nd 0.55 (XRD)
Space group		*Pbnm*	*Pbnm*	*Pbnm*	*Pbnm*
	x	−0.000(3)	−0.005(3)	−0.002(3)	−0.004(5)
Na/*Ln*	*y*	−0.017(2)	−0.016(2)	−0.021(3)	−0.021(4)
	z	0.250	0.250	0.250	0.250
	B (Å^2)	0.488(2)	0.696(3)	0.356(2)	0.849(1)
	x	0.500	0.500	0.500	0.500
Mn/Ti	*y*	0.000	0.000	0.000	0.000
	z	0.000	0.000	0.000	0.000
	B (Å^2)	0.270(2)	0.396(4)	0.099(1)	0.978(2)
	x	−0.050(1)	−0.064(1)	−0.080(4)	−0.077(3)
O1	*y*	0.511(8)	0.511(8)	0.516(5)	0.447(6)
	z	0.250	0.250	0.250	0.250
	B (Å^2)	1.357(4)	0.886(1)	0.487(3)	0.203(1)
	x	0.745(4)	0.733(4)	0.740(5)	0.750(1)
O2	*y*	0.264(2)	0.271(2)	0.275(6)	0.266(6)
	z	−0.030(1)	−0.028(1)	−0.025(4)	0.021(3)
	B (Å^2)	1.380(2)	0.886(1)	0.487(3)	0.203(1)
a (Å)		5.4539(6)	5.441(1)	5.438(8)	5.426(1)
b (Å)		5.4490(3)	5.440(4)	5.457(7)	5.435(6)
c (Å)		7.6944(3)	7.713(6)	7.680(9)	7.694(4)
V (Å^3)		228.660	228.305	227.884	226.91
R_B (%)		6.90	5.87	6.71	6.70
R_P (%)		6.25	5.78	11.1	9.58
R_{WP} (%)		6.51	12.5	16.1	14.2

The structure is built up from (Ti/Mn)O_6 octahedra and (*Ln*/Na)O_8 bicapped prisms and both kinds of polyhedra are related to the tilting of the BO_6 octahedra on the [001] and [110] directions of the parent structure (see inset in Fig. 1). The bending of the *B*–O–*B* angles is used to evaluate such a tilting and this factor is important in order to interpret the physical properties of the title materials, as is discussed below.

TABLE 2
Interatomic Distances (Å) and Angles (°) for BO_6 and AO_8 Polyhedra in $Ln_{1.33}Na_xMn_xTi_{2-x}O_6$

	Pr 0.66 (ND)	Pr 0.66 (XRD)	Nd 0.66 (XRD)	Nd 0.55 (XRD)
d(*B*–O1)	1.925(0) (×2)	1.956(0) (×2)	1.971(1) (×2)	1.989(4) (×2)
d(*B*–O2)	1.911(9) (×2)	1.960(8) (×2)	1.884(2) (×2)	1.865(3) (×2)
	2.000(2) (×2)	1.931(1) (×2)	1.996(0) (×2)	1.990(1) (×2)
Mean	1.945	1.949	1.950	1.948
Shannon	*2.018*	*2.018*	*2.018*	*2.018*
B–O1–*B*	159.1 (×2)	153.9 (×2)	153.9(8) (×2)	150.4(4) (×2)
B–O2–*B*	162.6 (×2)	169.5 (×2)	166.1(0) (×2)	169.7(2) (×2)
Mean	160.85	163.2	159.9	160.1
d(*A*–O1)	2.589(3)	2.597(1)	2.301(9)	2.356(4)
	2.301(2)	2.356(8)	2.566(9)	2.352(7)
d(*A*–O2)	2.509(3) (×2)	2.734(7) (×2)	2.544(0) (×2)	2.580(9) (×2)
	2.514(3) (×2)	2.523(4) (×2)	2.620(9) (×2)	2.610(9) (×2)
	2.867(2) (×2)	2.653(4) (×2)	2.726(1) (×2)	2.755(4) (×2)
Mean	2.583	2.597	2.581	2.575
Shannon	*2.540*	*2.540*	*2.527*	*2.462*

Electrical Properties

Measurements of a.c. impedance spectra have been carried out by alternating current techniques from the complex impedance (Z) graphs (11). Experimental data of Z'' (imaginary part) vs Z' (real part) at different temperatures (Fig. 2) show a semicircle and a spike at lower frequencies over the Z' axis that is characteristic of a conductivity process due to the electron motion. The capacitance for each sample is deduced from the respective maxima and is nearly constant with the temperature, being this quantity on the order of 9 pF. From these results we can assume that the response is exclusively due to the bulk of material and that contact phenomena can be neglected (12).

Conductivity values have been deduced from the intercept of the extrapolated high-frequency semicircles with the real impedance axis and they can be fitted to an Arrhenius equation of the form $\sigma = \sigma_o \cdot \exp(-E_a/kT)$, as is shown in Fig. 3. The activation energies values obtained from the a.c.

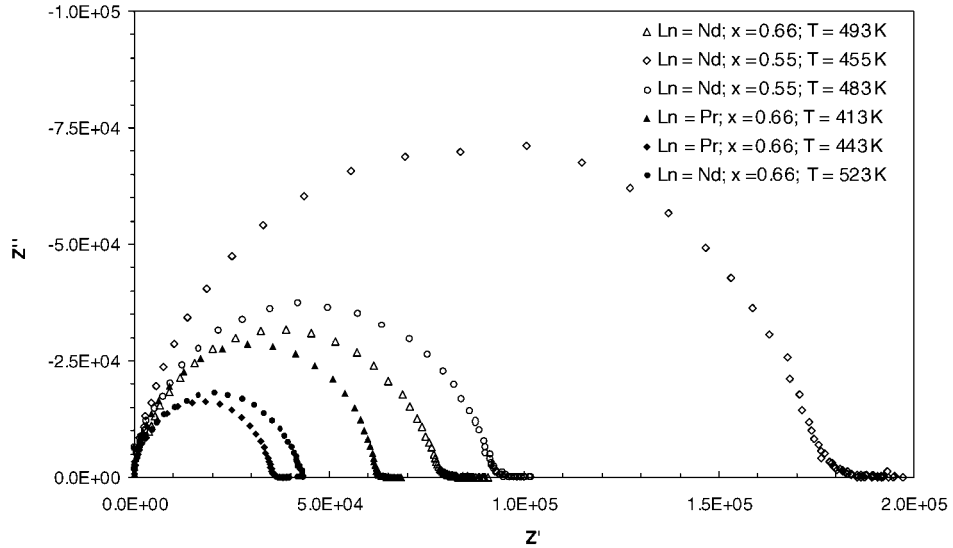

FIG. 2. Complex impedance plots at different temperatures for $Ln_{1.33}Na_xMn_xTi_{2-x}O_6$.

measurements are relatively low (of about 0.30 eV) and the temperature dependence of conductivity allow one to conclude that these materials behave as semiconductors. Moreover, the results of d.c. measurements (not shown) are very similar to those supplied by a.c. technique, suggesting that these materials are electronic conductors. On the other hand, polarization experiments were carried out following the method described in (5). The ionic transport number deduced was zero for all the samples thus confirming the exclusive electronic contribution to conductivity process.

Effectively, taking into account the above structural results, for the composition $x = 0.66$ the A sites are completely filled by Ln^{3+} and Na^+ cations and the movement of these latter ions throughout the structure is prevented. Comparison of conductivities for Pr and Nd phases shows that their behaviors are quite similar and the little Mn^{4+} content in the lower substituted Nd compound ($x = 0.55$) does not affect this quantity.

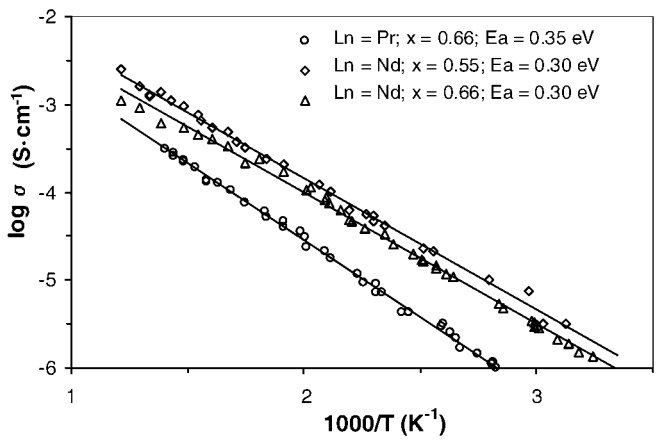

FIG. 3. Arrhenius plots for the sample $Ln_{1.33}Na_xMn_xTi_{2-x}O_6$.

Magnetic Behavior

Magnetic measurements were carried out on the Pr and Nd samples with higher compositions ($x = 0.66$) and Fig. 4 shows the temperature dependence of magnetic susceptibility (left scale) and its reciprocal (right scale). It can be observed that the reciprocal susceptibility follows a Curie–Weiss behavior between 150 and 300 K for the praseodymium sample and between 100 and 300 K for the neodymium sample. The experimental magnetic moments were 6.19 μ_B (Pr phase) and 6.15 μ_B (Nd phase), which are somewhat higher than the expected moments, 5.77 μ_B and 5.82 μ_B respectively, calculated from the contribution of free ions ($Mn^{3+} = 4.90$, $Pr^{3+} = 3.62$, and $Nd^{3+} = 3.68$, in μ_B). On the other hand, the Weiss constant gave positive values, 112 and 20 K for Pr and Nd samples, respectively,

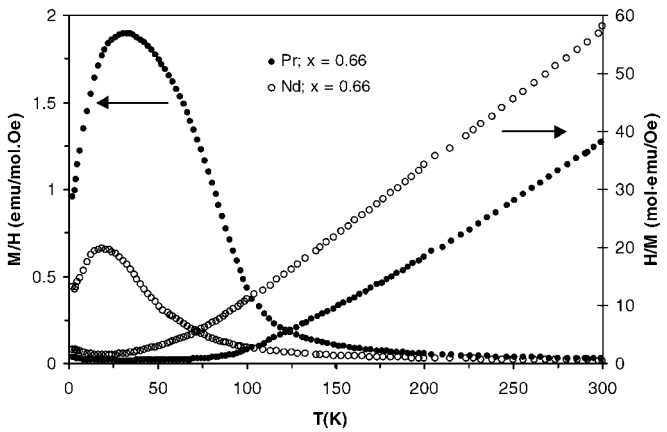

FIG. 4. Susceptibility and reciprocal susceptibility variation for $Ln_{1.33}Na_{0.66}Mn_{0.66}Ti_{1.34}O_6$.

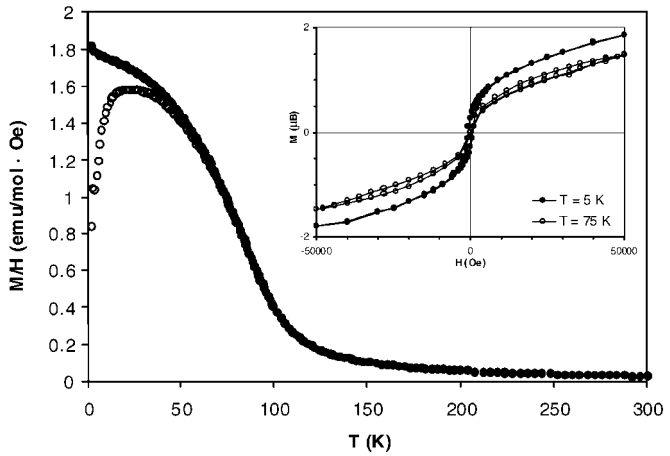

FIG. 5. (a) Magnetization vs magnetic field for $Pr_{1.33}Na_{0.66}Mn_{0.66}Ti_{1.34}O_6$. (b) (filled symbols) ZFC and (open symbols) FC measurements for $Pr_{1.33}Na_{0.66}Mn_{0.66}Ti_{1.34}O_6$.

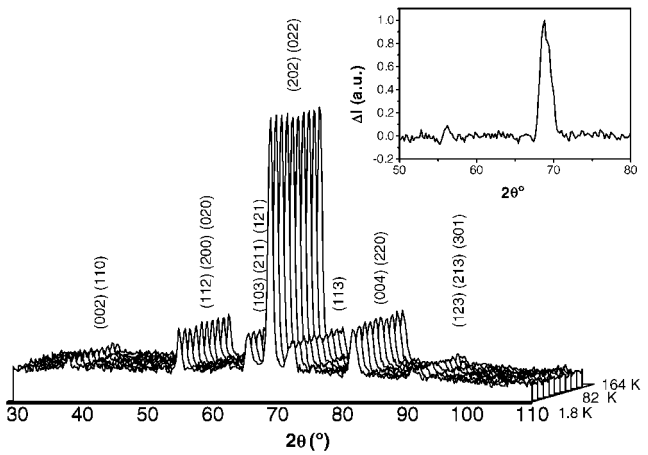

FIG. 6. Neutron thermodiffractograms of $Pr_{1.33}Na_{0.66}Mn_{0.66}Ti_{1.34}O_6$ between 1.8–164 K and angular range 30–110° and difference pattern diffraction between 1.8 and 164 K (inset).

suggesting again that cooperative magnetic interactions are present in both compounds.

In order to clarify the magnetic behavior of this system, isotherms at 5 and 75 K for $Pr_{1.33}Na_{0.66}Mn_{0.66}Ti_{1.34}O_6$ were obtained (Fig. 5a). The narrow hystheresis loops observed indicate that this material behaves as a weak ferromagnet being the values of the magnetic moment 1.0 μ_B (5 K) and 0.75 μ_B (75 K). The low values of the magnetization could be explained by recalling that Mn^{3+} ions on *B* sites are randomly distributed together with diamagnetic Ti^{4+} ions, which prevents the establishment of the long-range order in the whole sample (13). Moreover, the hystheresis observed in the graphs of magnetization (Fig. 5b) obtained at zero field cooled (ZFC) and field cooled (FC) suggests a random system of ferromagnetic clusters with a freezing temperature of 50 K (14). Typical spin–glass transitions are due to the existence of different exchange interactions that are competing and hence giving rise to a certain degree of magnetic frustration (15). This is usually found in disordered structures and it has been particularly observed in $AB_{1-x}B'_xO_3$ perovskites when some degree of disorder at the *B* site is achieved for the magnetic ion (16). In this compound, where the ratio Ti^{4+}/Mn^{3+} is 2, the system is magnetically diluted and is reasonably the occurrence of the spin–glass transition.

Neutron diffraction experiments were performed to confirm the origin of the ferromagnetism in $Pr_{1.33}Na_{0.66}Mn_{0.66}Ti_{1.34}O_6$. Figure 6 shows some thermodiffractograms at low temperature of this compound and one can notice that below a $T_c = 82$ K a weak ferromagnetic contribution appears on the (020/112) and (202/022) Braggs peaks. This contribution is very small (inset Fig. 6) so that it was not possible to obtain a ferromagnetic component. Results suggest that there is not any long-range magnetic contribution and they agree with the above data on the existence in this system of a cluster-glass state at low temperatures, in which ferromagnetic clusters are randomly orientated (16). In order to gain a deeper insight in the spin–glass behavior of this oxide, we have performed χ_{ac} measurement as a function of temperature at different frequencies (Fig. 7). In this figure, it is shown that the real part of χ_{ac} exhibits a maximum at 62 K, which is decreased in intensity as the frequency of the measurement is increased from 1 to 1000 Hz, as described in literature for spin–glasses (17).

By comparing previous results (5) in the related system $La_{1.33}Na_xMn_xTi_{2-x}O_6$ (phases noted as La-*x*) with present compounds (*Ln*-*x*) some interesting features appear. From the structural point of view, a change in symmetry was observed in the La phases: La-0.66 is orthorhombic (s.g. *Pbnm*), whereas La-0.55 is rhombohedral (s.g. $R\bar{3}c$) at room temperature, being orthorhombic (s.g. *Pbnm*) for Pr and Nd. In the La-*x* derivatives larger cations occupy sites with

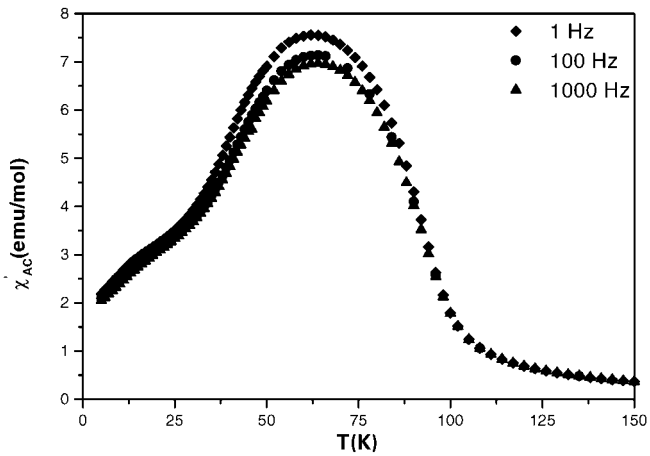

FIG. 7. Thermal dependence of the ac susceptibility at different values of the excitation frequency.

c.n. = 12 in both space groups but in the Pr and Nd phases the c.n. is lowered to 8 because of the greater tilting of BO_6 octahedra. On the other hand, for $x = 0.66$ the A sites are completely occupied in all cases and this absence of vacancies hinders the ionic mobility, causing these phases to behave as purely electronic conductors. The remaining La-0.55 and La-0.44 derivatives are mixed ionic–electronic conductors but only Ln-0.55 shows an electronic contribution. This fact could be attributed to the above structural distortion, keeping in mind that ionic motion is blocked as a consequence inherent to the lower size in A sites. Finally, magnetic behavior of the title compounds is similar to that observed in the La-x system (which will be reported in due course) and implies the exclusive interactions between manganese cations.

ACKNOWLEDGMENTS

We are indebted to the CICYT (Grant MAT2000-1585-C03-02) for financial support. We acknowledge the ILL (CRG-D1B) for collecting data of neutron diffraction. One of authors (A.I.R.) is grateful to the CAM for a "beca predoctoral".

REFERENCES

1. C. N. R. Rao and A. K. Cheetham, *Adv. Mater.* **9,** 1009 (1997).
2. J. Rodriguez-Carvajal, M. Hennion, F. Moussa, A. H. Moudden, L. Pinsard, and A. Revcolevschi, *Phys. Rev. B* **57,** R3189 (1998).
3. J. P. Attfield, *Chem. Mater.* **10,** 3239 (1998).
4. M. Marezio, P. D. Dernier, and J. P. Remeika, *J. Solid State Chem.* **4,** 11 (1972).
5. A. I. Ruiz, M. L. López, M. L. Veiga, and C. Pico, *Eur. J. Inorg. Chem.* 659 (2000).
6. M. Pechini, U.S. pattent 3, 231, 328 (1966).
7. I. Alvarez, M. L. Veiga, and C. Pico, *J. Alloys Comp.* **255,** 74 (1997).
8. E. O. Wollan and W. C. Foehler, *Phys. Rev.* **100**(2), 545 (1955).
9. J. Rodriguez Carvajal, *Physica A* **192B,** 55 (1993).
10. J. Töpfer and J. B. Goodenough, *J. Solid Sate Chem.* **130,** 117 (1997).
11. "Zview, Graphics and Analysis Software," Scriber Associates 1994.
12. H. H. Sumathipala, M. A. K. L. Dissanayake, and A. R. West, *Solid State Ionics* **86,** 719 (1996).
13. C. N. R. Rao and B. Raveau "Colossal Magnetoresistance, Change Ordering and Related Properties of Manganese Oxides." Word Scientific, Singapore, 1998.
14. B. C. Hanback, F. Helemer, and N. Sakai, *J. Solid State Chem.* **124,** 43 (1996).
15. K. Moorjani and J. M. D. Coey, "Magnetic Glasses." Elsevier, Amsterdam 1984.
16. V. Primo-Martín and M. Jansen, *J. Solid State Chem.* **157,** 76 (2001).
17. J. A. Mydosh, "Spin Glasses: An Experimental Introduction," Taylor and Francis, London, 1993.